Characterisation of the superconducting properties of NbN and TiN thin films

Simultaneous measurements on multiple samples

Olivia Armitage, Ben Yager

1. Background

NbN and TiN are materials of increasing interest for the manufacture of quantum devices [1] [2].

In particular TiN is of interest due to its tuneable superconducting properties, chemical stability and compatibility with high volume manufacturing. Hence TiN films are being investigated for superconducting quantum applications, such as for sensing [3] or computing [4] [5] [6]. For these applications the film quality (crystallinity, low-contamination levels, thickness control) is imperative to ensure functionality and optimal performance in the final device.

The temperature dependence of the resistivity and the superconducting transition temperature, T_C, for thin film samples of NbN and TiN are presented. From sheet resistivity measurements at room temperature and at 20 K, the residual resistivity ratio values for the samples are also determined.

The TiN samples were prepared using Plasma Enhanced Atomic Layer Deposition (PEALD) by Oxford Instruments Plasma Technology (OIPT) using their PlasmaPro ASP [7]. These films were deposited to a thickness of 95 ± 5 nm. By optimising the PEALD process, films with high superconducting transition temperatures and low resistivities can be deposited [1].

To investigate the impact of different process conditions on film properties we also make measurements of two NbN films, the results of which serve as input for continuous internal process optimisation at OIPT. Further details on the atomic layer deposition of NbN and TiN with the PlasmaPro ASP can be found in [8] [9].

All samples had other dimensions $\sim 3 \times 3$ mm.

Utilising the large quantity of user accessible wiring on the **Teslatron**PT Plus measurement probes [10], all four samples are able to be measured simultaneously; greatly increasing laboratory throughput.

2. Methods

The measurements were made using the **Teslatron**PT Plus system. Lake Shore measurement instrumentation was used to determine the resistance and/or resistivity of the samples.

The resistances were calculated from a four-point (AC) lock-in measurement from the M81-SSM synchronous source measure system [11], while the sheet resistivity was determined from van der Pauw measurements [12] using the M91 FastHall™ measurement controller [13].

During temperature-dependent measurements, all four samples were measured simultaneously, with the resistivity of one sample measured with the M91 controller, and the resistances of the others using

[1] For additional details on the PEALD process please refer to the recent blog post from Oxford Instruments Plasma Technology High T_c TiN using plasma enhanced ALD.

three sets of current source (BCS-10) and voltage measure (VM-10) units attached to a M81 mainframe (the lock-in frequency for each sample being different at 13, 17 and 19 Hz respectively).

The measurements were automated using QCoDeS [14] Python scripts that utilised instrument drivers for the Lake Shore instrumentation and the **Teslatron**PT Plus system.

3. Results

3.1. Room temperature sheet resistivity

The sheet resistivities of the samples measured with the M91 controller at room temperature (approximately 296 K) are given in table 1. The corresponding errors are the standard error values reported by the M91 controller from 50 readings.

The sheet resistivity values are constant for a range of excitation currents (see section A.1). However, the error in the measurement increases significantly for smaller currents, accompanied by a decrease in the signal-to-noise ratio. A value of 0.2 mA is chosen for most of the subsequent measurements as a compromise between the effects of self-heating (especially at lower temperatures, see section A.4) and the standard error in the reported resistivity.

Sample	Material	Sheet resistivity ($\Omega\square^{-1}$)
A	TiN	6.99581 ± 0.00008
B	TiN	5.14112 ± 0.00008
C	NbN	40.9326 ± 0.0001
D	NbN	31.94778 ± 0.00008

Table 1: Sheet resistivity measurements at room temperature (296 K). Each value is the average of 50 readings with an excitation current of 0.2 mA

3.2. Temperature dependence of resistivity/resistance

The samples were cooled over approximately 48 hours from room temperature to a base temperature of ~ 1.8 K. In figure 1 the resistivity/resistance measurements of the samples during the cooldown are shown. The resistances of the TiN samples (A and B) decrease linearly with temperature until temperatures of around 120 K and 130 K respectively. The resistance of sample D also decreases with

temperature, but that of sample C increases to a maximum value around 65 K, before decreasing as it cools further.

The superconducting transition of all samples was also identified; this is discussed further in section 3.4.

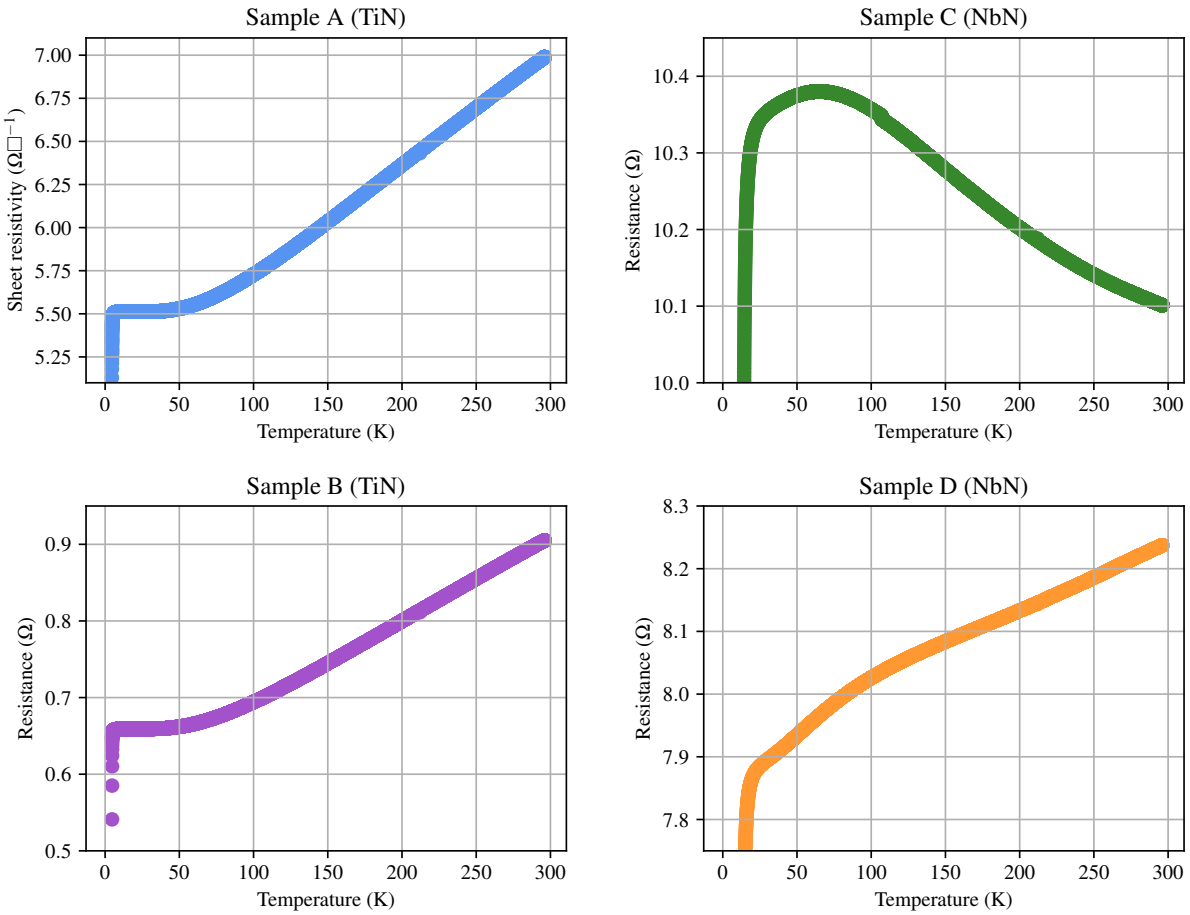

Figure 1: Sheet resistivity (sample A) and resistance (samples B-D) measurements as a function of temperature during cooldown, over a time period of about 48 hours. An excitation current of 0.2 mA was employed for both the resistivity and resistance measurements. Each sheet resistivity value (sample A) is an average of 10 readings.

3.3. 20 K sheet resistivity measurements

The sheet resistivity measurements, using the M91 controller, were repeated at 20 K. The resulting sheet resistivity values are given in table 2.

The errors in the measurements remain approximately unchanged from the room temperature mea-

surements. As with the room temperature measurements, the 20 K sheet resistivity shows no clear dependence on the excitation current, when taking into account the increasing error in the value as the current is decreased (see figure 6).

Sample	Sheet resistivity ($\Omega\square^{-1}$)
A	5.51237 ± 0.00008
B	3.74109 ± 0.00008
C	41.8265 ± 0.0001
D	30.5012 ± 0.0001

Table 2: Sheet resistivity measurements at 20 K. Each value is from an average of 50 samples with an excitation current of 0.2 mA.

3.3.1. Residual resistivity ratio

The Residual Resistivity Ratio (RRR) value is often used as a yardstick to assess the level of impurities and/or crystallographic defects present in a sample. Given the high T_C of the samples used in this work it is defined in this case as:

$$RRR = \frac{\rho_s(296\ \mathrm{K})}{\rho_s(20\ \mathrm{K})}$$

Where $\rho_s(T)$ is the resistivity of the sample at temperature T.

The calculated value for each sample is given in table 3. The RRR values for each sample is close to 1. This specific measurement is most relevant to the TiN samples where the sheet resistivity plateaus below approximately 50 K. There is still a significant temperature dependence of sheet resistivity at 20 K for the NbN samples, however those data are still included for completeness. For sample C the resistivity ratio remains greater than 1 until T_C.

Sample	RRR
A	1.26911 ± 0.00002
B	1.37423 ± 0.00004
C	0.9786295 ± 0.000003
D	1.0474284 ± 0.000004

Table 3: RRR values calculated from sheet resistivity measurements at room temperature (296 K) and 20 K.

3.4. Superconducting transition temperatures

The superconducting transitions of all four samples are shown in figure 2. The transition temperatures of the NbN samples are similar (at 13.872 ± 0.001 and 14.129 ± 0.001 K), as are those for the TiN samples (at 4.583 ± 0.002 and 4.700 ± 0.002 K). The superconducting transitions are narrower for the TiN samples, taking place over a temperature range an order of magnitude smaller than for the NbN ones.

Previous work has shown that reducing film thicknesses below ~ 150 nm leads to an exponentially decreasing T_C for TiN films [15], and so the results presented here for ~ 95 nm films demonstrate the high quality of the deposition.

When plotted over a smaller temperature range, as in figure 3, a difference between increasing and decreasing temperature sweeps can be seen. Since the transition width of the TiN samples is narrower than that for the NbN ones, a lower sweep rate was used in order to acquire sufficient data in this temperature range. In these cases, the results from increasing and decreasing temperature sweeps are indistinguishable; with the main error in identifying T_{50} being due to fluctuations in the sample resistance rather than any temperature lagging (discussed further in appendix section A.3). This is not the case for the NbN samples where there is a clear distinction between the two temperature sweeps. Slower sweeps over the narrower temperature range in which the transition occurs are shown in figure 7 for samples C and D and in figure 8 for sample A. Since the increasing temperature sweep in figure 3 is consistent with these slow sweeps (as discussed in appendix section A.2), these data are used in estimating the transition temperature and width.

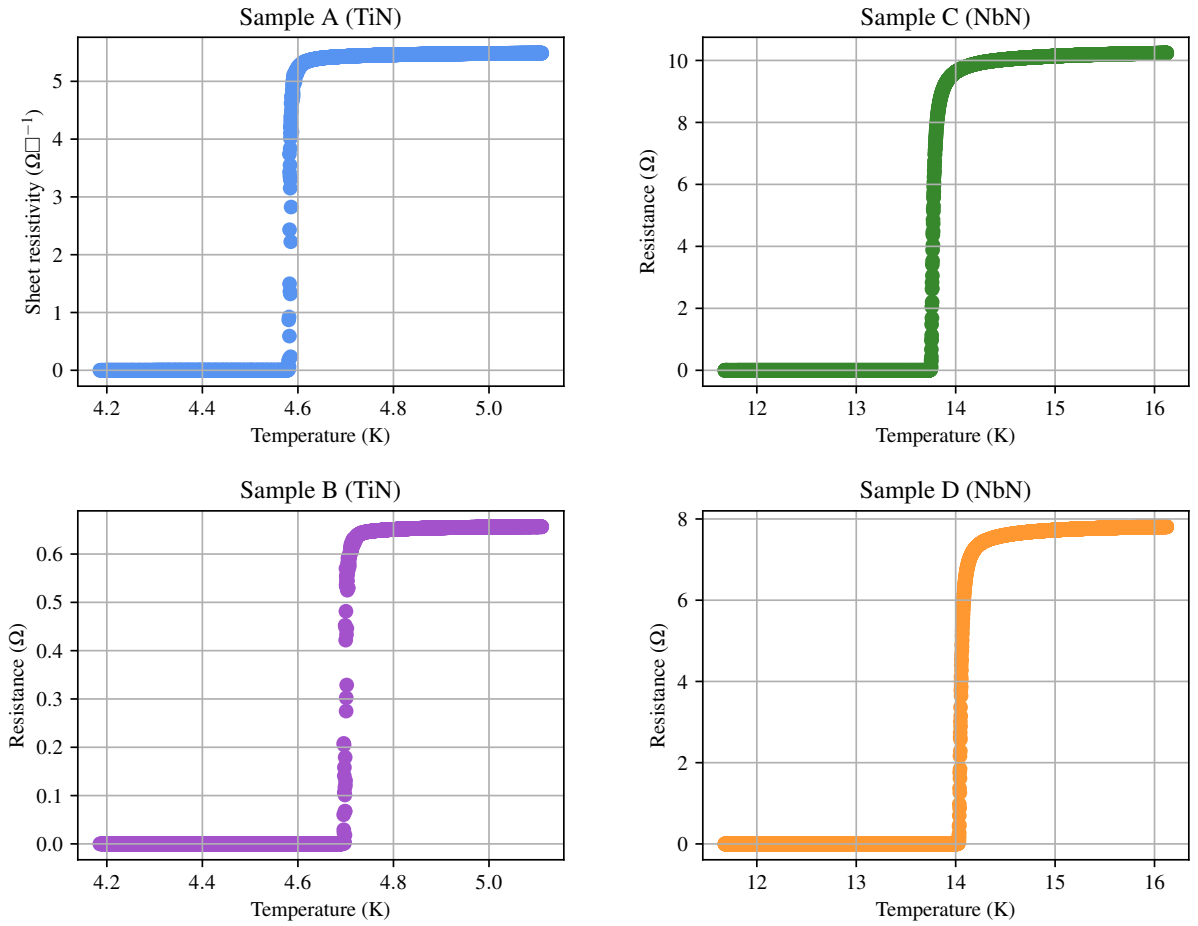

Figure 2: Superconducting transitions of the samples. Temperature ramp rates $\sim 3.3 \times 10^{-5}$ K s^{-1} for samples A and B, $\sim 1.7 \times 10^{-4}$ K s^{-1} for samples C and D. Increasing and decreasing temperature sweeps are both plotted. An excitation current of 0.2 mA was employed for all measurements. Each sheet resistivity value (sample A) is an average of 10 readings.

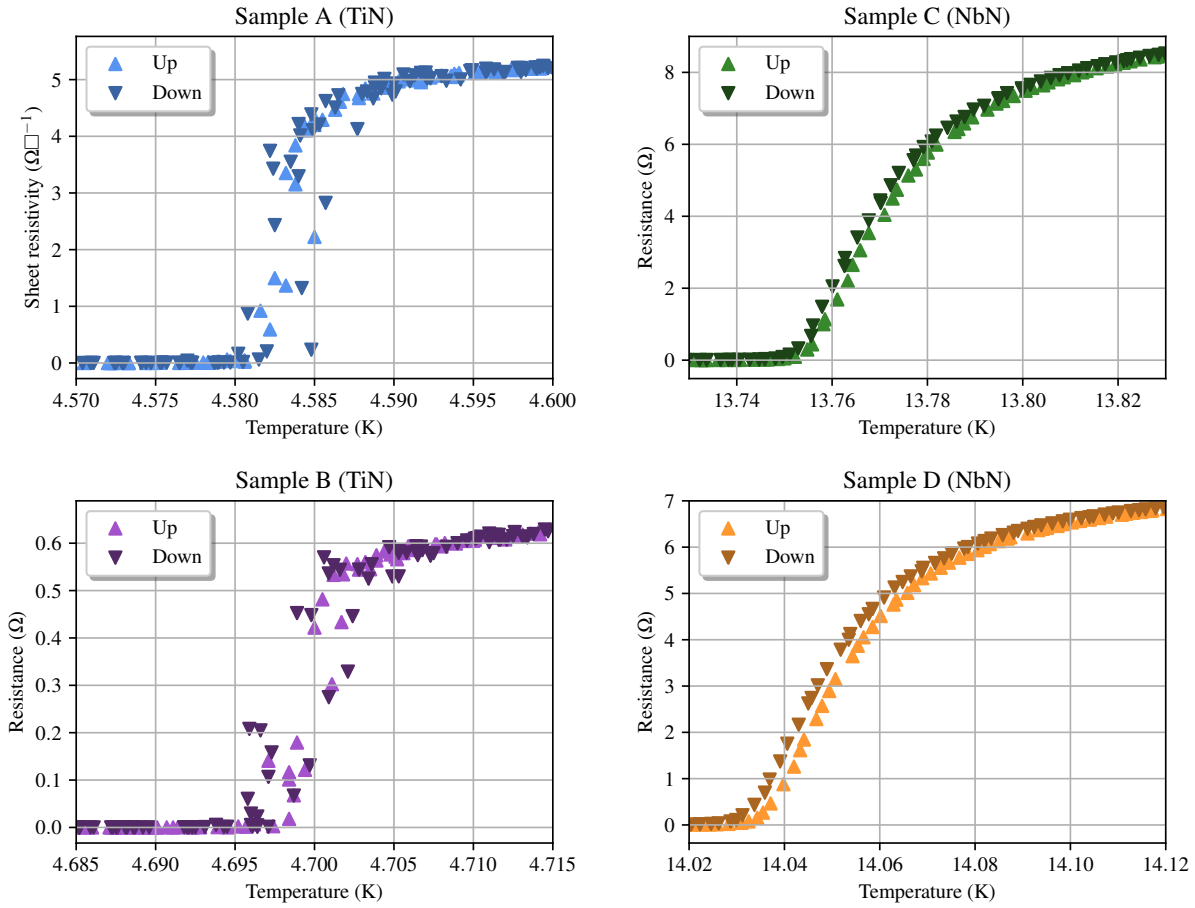

Figure 3: Superconducting transitions of the samples, the data presented in figure 2 here plotted over a narrower temperature range, showing the increasing (up) and decreasing (down) temperature sweeps. Ramp rates $\sim 3.3 \times 10^{-5}$ K s^{-1} for samples A and B, $\sim 1.7 \times 10^{-4}$ K s^{-1} for samples C and D. An excitation current of 0.2 mA was employed for all measurements. Each sheet resistivity value (sample A) is an average of 10 readings.

T_C is defined as the temperature at which the resistance of the samples is 50% of its normal-state value (denoted as T_{50}). Since the normal state resistance also varies with temperature (as can be seen in figure 2), a straight line is fitted to the data above the superconducting transition and a similar line, with the same gradient but half the resistivity/resistance values, is used to determine T_{50}. Corresponding lines with 90% and 10% of the normal-state resistivity/resistance values are used to find T_{90} and T_{10}, the difference between which defines the transition width. An example of the fitting procedure used for the analysis is shown in figure 4 for sample C.

Applying this analysis to the data shown in figure 2 gives the values of T_C and transition width reported in table 4.

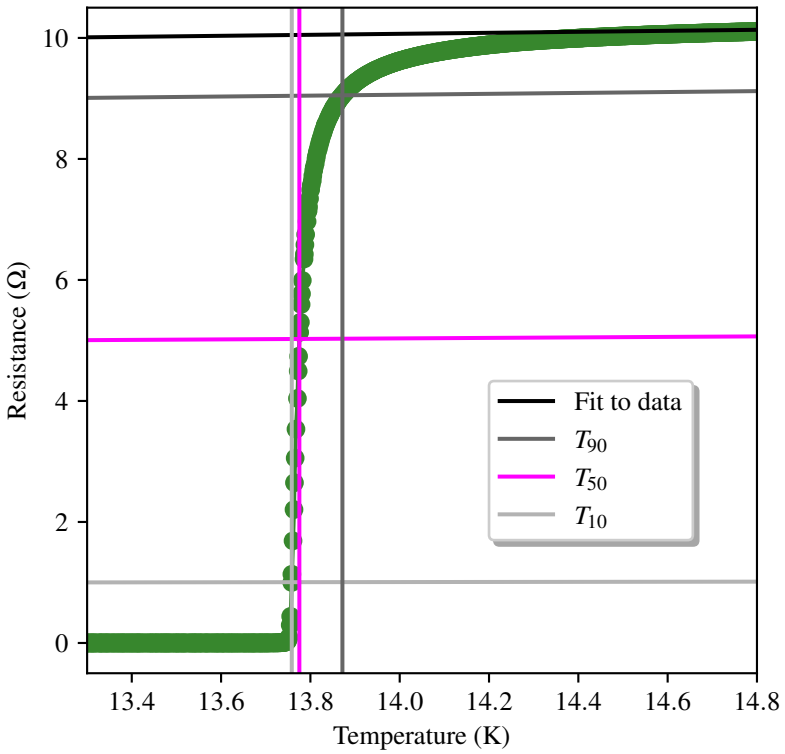

Figure 4: Superconducting transition temperature and width analysis for sample C, using the upwards temperature ramp data from figure 2 (ramp rate $\sim 1.7 \times 10^{-4}$ K s^{-1}). The black line shows a fit to those data between the transition and 16.1 K, with the lower temperature cut-off for the fit chosen such that the R-value is above 0.99. The dark grey, magenta and light grey near-horizontal lines have the same functional form as the black line, but with 90%, 50% and 10% of the resistance values. The points where these lines intersect with the measured resistance data determine T_{90}, T_{50} and T_{10}, shown by the dark grey, magenta and light grey vertical lines. T_{50} is the value of T_C, while $T_{90} - T_{10}$ gives the transition width.

Sample	T_C (K)	T_{90} (K)	T_{10} (K)	Transition width (K)
A	4.583 ± 0.002	4.589 ± 0.002	4.582 ± 0.002	0.007 ± 0.003
B	4.700 ± 0.002	4.706 ± 0.002	4.699 ± 0.002	0.007 ± 0.003
C	13.775 ± 0.001	13.872 ± 0.001	13.758 ± 0.001	0.114 ± 0.001
D	14.055 ± 0.001	14.129 ± 0.001	14.039 ± 0.001	0.090 ± 0.001

Table 4: Superconducting transition temperature ($T_C = T_{50}$) and transition width ($T_{90} - T_{10}$) for each sample. The analysis method demonstrated in figure 4 is applied to the data from figure 2 to provide these values.

The critical surface of a superconductor is a function of temperature, field and current [16], this means for all the samples there may also be an error in the transition temperature due to its dependence on the applied current. The effects of the excitation current on the superconducting transition are discussed in section A.4. For currents up to 1 mA, the change in transition temperature is of the order of a few mK and the change in the transition width correspondingly small. Hence the values given in table 4 are believed to be close to the true T_C.

4. Conclusions

Confirmation of the superconducting nature of the TiN films indicates that PEALD is a viable approach for quantum materials processing. The high T_C, narrow transition width, and RRRs observed indicates the high quality of the film and that there is minimal contamination.

Combining the inherent qualities of ALD (nm-scale control, conformality and wafer-scale thickness uniformity) with the ability to precisely tune material properties will be enabling for future quantum device fabrication.

It was possible to make four, simultaneous electrical-transport measurements using the **Teslatron**PT Plus platform; demonstrating the potential for high-throughput characterisation of samples at low temperatures. The system has an intrinsically low noise-level allowing excitation currents to be kept sufficiently low to avoid sample self-heating. The excellent temperature stability means that temperature sweeps can be made at rates appropriate to avoid any thermal lag between the reported system temperature and the sample temperature.

References

[1] E. Mutsenik, S. Linzen, E. Il'ichev, M. Schmelz, M. Ziegler, V. Ripka, B. Steinbach, G. Oelsner, U. Hübner, and R. Stolz, Superconducting $\mathrm{NbN} - \mathrm{Al}$ hybrid technology for quantum devices, Low Temperature Physics **49**, 92 (2023).

[2] S. Bugu, S. Biradar, A. Blake, C. Liu, M. Myronov, R. Duffy, G. Fagas, and N. Petkov, High-fidelity TiN processing modes for multigate Ge-based quantum devices, ACS Applied Electronic Materials **7**, 652 (2025).

[3] E. Schroeder, P. Mauskopf, H. Mani, S. Bryan, K. K. Berggren, and D. Zhu, Operation of a superconducting nanowire in two detection modes: KID and SPD, Journal of Low Temperature Physics **194**, 386 (2019).

[4] K. Grigoras et al., Qubit-compatible substrates with superconducting through-silicon vias, IEEE Transactions on Quantum Engineering **3**, 1 (2022).

[5] A. Bozkurt, H. Zhao, C. Joshi, H. G. LeDuc, P. K. Day, and M. Mirhosseini, A quantum electromechanical interface for long-lived phonons, Nature Physics **19**, 1326 (2023).

[6] A. Schewski, U. Schaber, and A. Klumpp, *Superconducting Titanium Nitride in Through-Silicon Vias for 3D Integration of Qubits*, in *2024 International 3D Systems Integration Conference (3DIC)* (2024), pp. 1–6.

[7] Plasma Pro ASP, (https://plasma.oxinst.com/products/ald/plasmapro-asp).

[8] N. Choudhary, S. A. Peeters, C. T. Lennon, D. Besprozvannyy, H. C. M. Knoops, I. Maclaren, and R. H. Hadfield, Transmission electron microscopy analysis of atomic layer deposited $\mathrm{NbTiN}/\mathrm{NbN}$ superconducting thin films, APL Materials **13**, 111104 (2025).

[9] S. A. Peeters et al., Superconducting $\mathrm{Nb}_x\mathrm{Ti}_{1-x}\mathrm{N}$ prepared at high deposition rates with plasma-enhanced atomic layer deposition and substrate biasing, AVS Quantum Science **7**, 026801 (2025).

[10] TeslatronPT Plus, (https://qd-oxford.com/products/teslatronPT_Plus.html).

[11] M81-SSM synchronous source measure system, (https://www.lakeshore.com/).

[12] L. J. van der Pauw, A method of measuring the specific resistivity and Hall effect of discs of arbitrary shape, Philips Research Reports **13**, 1 (1958).

[13] M91 FastHall measurement controller, (https://www.lakeshore.com/).

[14] QCoDeS data acquisition framework, (https://microsoft.github.io/Qcodes/).

[15] M. I. Faley, Y. Liu, and R. E. Dunin-Borkowski, Titanium nitride as a new prospective material for NanoSQUIDs and superconducting nanobridge electronics, Nanomaterials **11**, (2021).

[16] M. N. Wilson, *Superconducting Magnets* (Oxford University Press, 1987).

A. Appendices

Some further technical details of the measurements presented are given in the following sections.

A.1. The dependence of sheet resistivity measurements on excitation current

To investigate the dependence of the sheet resistivity on the excitation current, measurements were taken with an M91 controller on sample A for values between 10 μA and 1 mA (shown in figures 5, 6 for room temperature and 20 K).

For the three highest current values (between 0.2 and 1 mA), the resistivities are similar; there is much more discrepancy as the excitation current is decreased. However, there does not appear to be a clear trend towards lower values at lower excitation currents, suggesting that any self-heating of the sample is not great enough to increase the sheet resistivity value considerably. The variation in the reported resistivity values across the different excitation ranges is consistent with the absolute accuracy (0.2%) of the calibration of the M91.

The value of 0.2 mA was chosen as the excitation current for the resistivity and resistance measurements as the lowest possible current (to minimise self-heating) without a significant standard error.

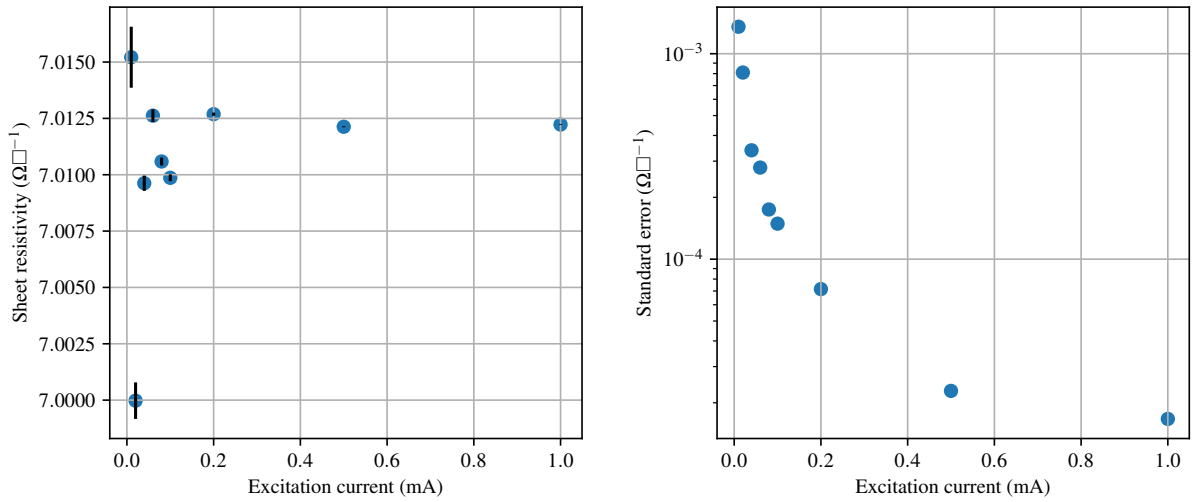

Figure 5: Sheet resistivity of sample A and the associated standard error as a function of excitation current at room temperature (approximately 296 K).

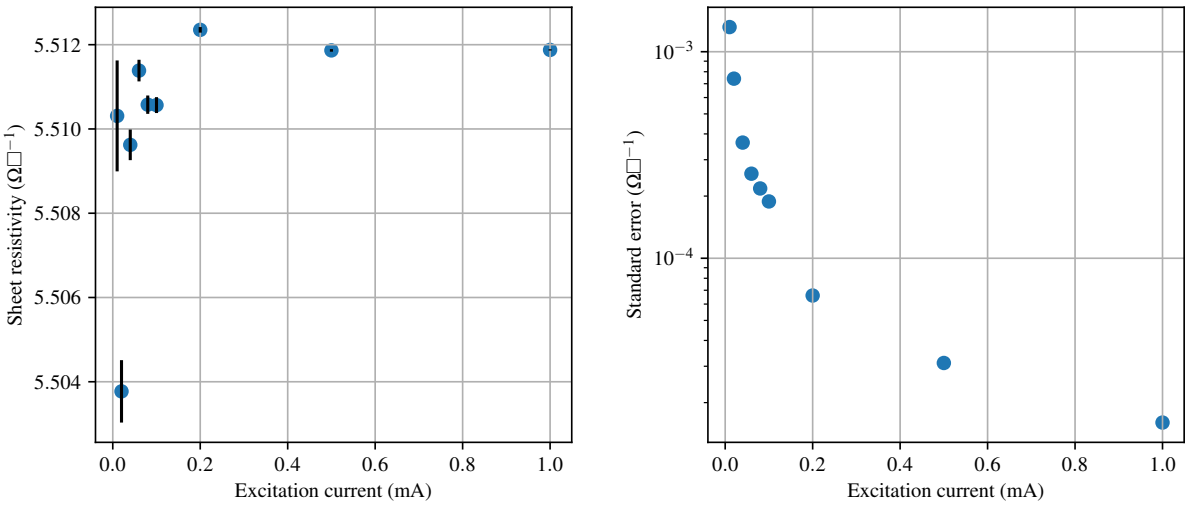

Figure 6: Sheet resistivity of sample A and the associated standard error as a function of excitation current at 20 K.

A.2. The effect of ramp rate on measured superconducting transition temperature

As the temperature is varied by the heater there will be some thermalisation process by which the surrounding probe (including the sample and the temperature sensor) reaches thermal equilibrium. This can cause inhomogeneity in the temperature at any given time. As a result, the rate at which the temperature is varied on the probe and the direction of the temperature ramp will affect the measured transition temperature of the sample. This is illustrated in figure 7, where temperature sweeps over the superconducting transitions of samples C and D with faster and slower ramp rates are shown.

For the faster ramp rate, there is a clear hysteresis in the resistance values, whereas the slower ramps measured on sample C are consistent with each other (within the error of temperature stability, about 1 mK).

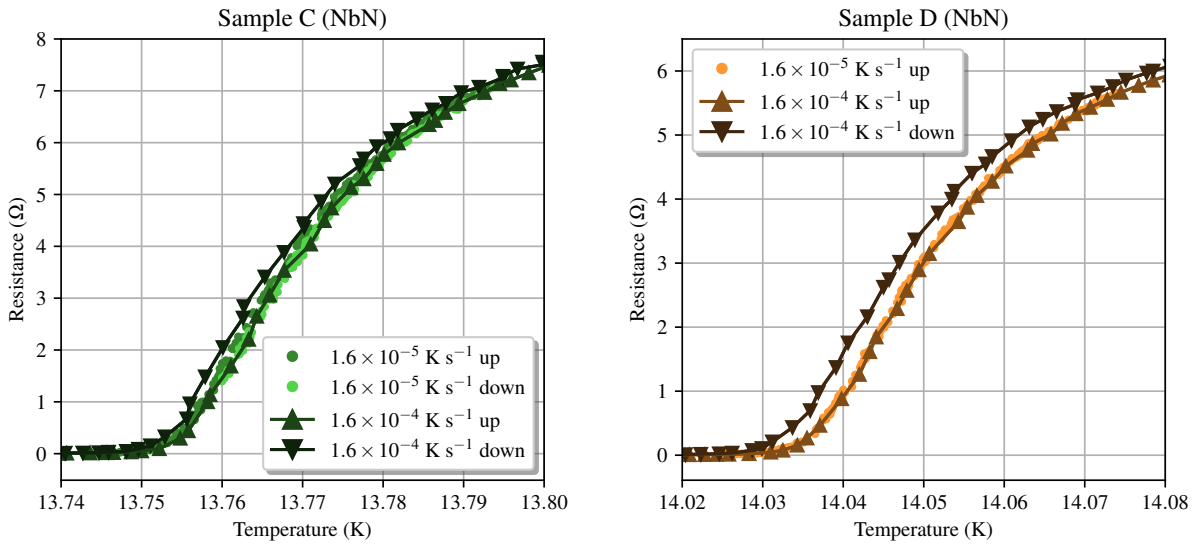

Figure 7: Temperature sweeps over the superconducting transitions of samples C and D with higher and lower ramp rates. The higher ramp rate data is the same as shown in figure 3. An excitation current of 0.2 mA was used for all measurements.

Given the much narrower transition for the TiN samples (figure 8), slower temperature ramp-rates were chosen to allow sufficient data to be acquired. This resulted in there being no observable effect of the ramp rate on the transition temperature, since both the faster upwards and downwards ramps are consistent with the slower ramp data.

For both sets of samples it is possible to ramp the temperature sufficiently slowly to ensure the system is well thermalised.

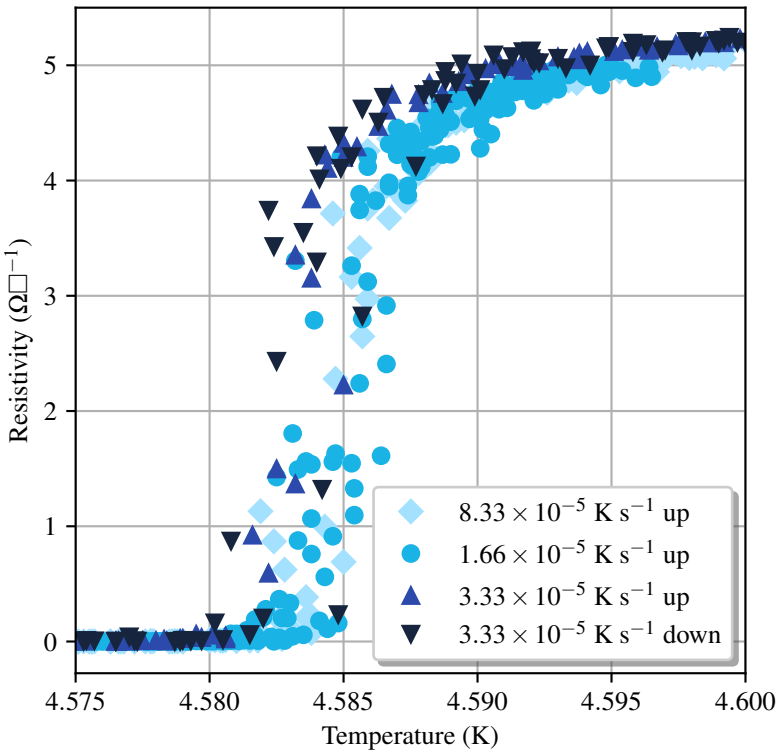

Figure 8: Temperature sweeps over the superconducting transition of sample A with higher and lower ramp rates. An excitation current of 0.05 mA was used for these measurements.

A.3. Resistance fluctuations at the superconducting transition

The superconducting transition of sample A is shown as a function of time in figure 9. Far away from the transition, either above or below, the variation in the resistivity is small. However during the transition the values can vary by several $\Omega\square^{-1}$, and are much larger than any corresponding fluctuation in sample temperature.

The critical current density, J_c, for TiN can be in excess of 10 MA cm^{-2} [15]. This means that, even for samples 95 nm thick, only a narrow channel is required to carry the 0.2 mA excitation current.

The evolution of the superconducting state is likely to have complex dynamics as small channels may initially become superconducting, only to then quench [16] as current from other regions of the sample is diverted through this lower resistance path, which in turn may lead to localised Joule heating, raising the sample resistance. This process would continue until there is a channel capable of carrying the full excitation current. During this time the measured potential difference across the sample (and hence inferred resistance/resistivity) would reflect these changes.

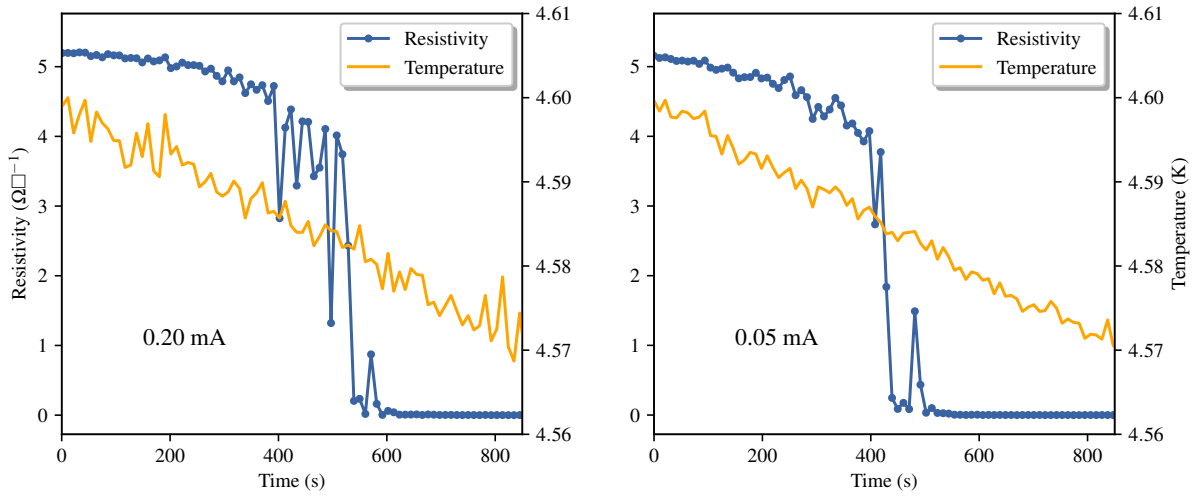

Figure 9: The resistivity of sample A, for two different excitation currents, plotted against time as the temperature is swept slowly. The measured temperature is also shown against time.

There could be some evidence to support this hypothesis from looking at the transition at lower excitation currents (where any Joule heating in a quenched channel would be correspondingly lower). The results shown in figure 9 measured at 0.05 mA excitation currents may show a lower level of fluctuations when compared to data recorded with a 0.2 mA excitation.

A.4. The dependence of superconducting transition temperature on excitation current

The magnitude of the current passed through a superconductor will have an effect on its superconducting transition temperature. Temperature sweeps across the transition applying 0.2 mA and 0.05 mA (figure 10) suggest that at these currents the effect is comparable to the other uncertainties in these data.

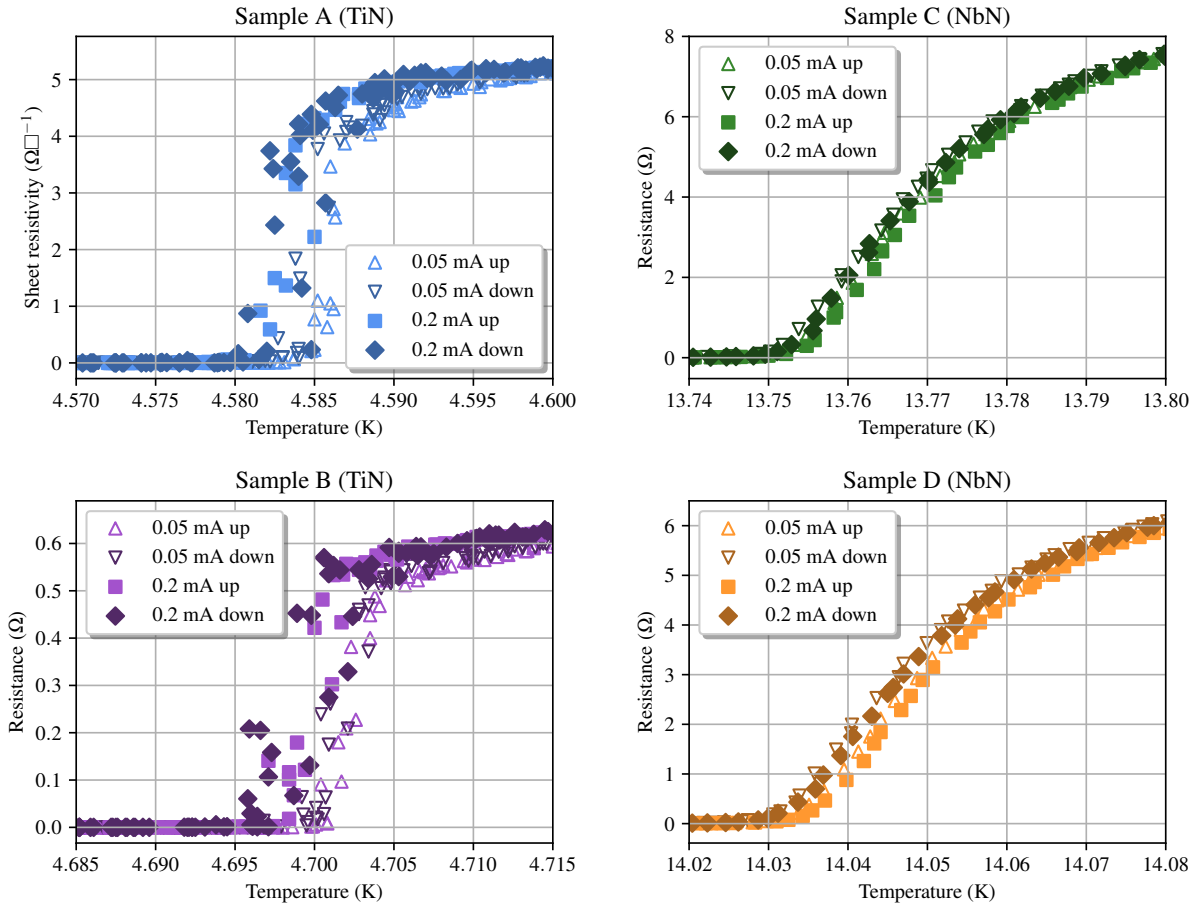

Figure 10: Effect of excitation current on the superconducting transitions of the samples. Ramp rates of $\sim 3.3 \times 10^{-5}$ K s^{-1} for samples A and B, $\sim 1.6 \times 10^{-4}$ K s^{-1} for samples C and D. Each sheet resistivity value (sample A) is an average of 10 readings.

The effect of higher excitation currents is investigated for sample C (in figure 11), since it has a broader transition than samples A and B. For a current of 1 mA, there is a significant difference in the transition temperature, as summarised in table 5.

When a sample becomes resistive, there will be Joule heating present ($\propto I^2R$). At higher excitation currents, there will be higher levels of dissipation that could lead to local self-heating within the sample. This is possibly shown in figure 11, where at the highest excitation current (1 mA) the resistance increases faster with temperature than for all the measurements made at lower excitations amplitudes.

The faster increase in resistance with temperature results in an associated change in the T_C determined at this current when compared to that determined at the lower excitations. The value of 0.2 mA selected for the measurements presented here appears to be below the level where self-heating would influence the results.

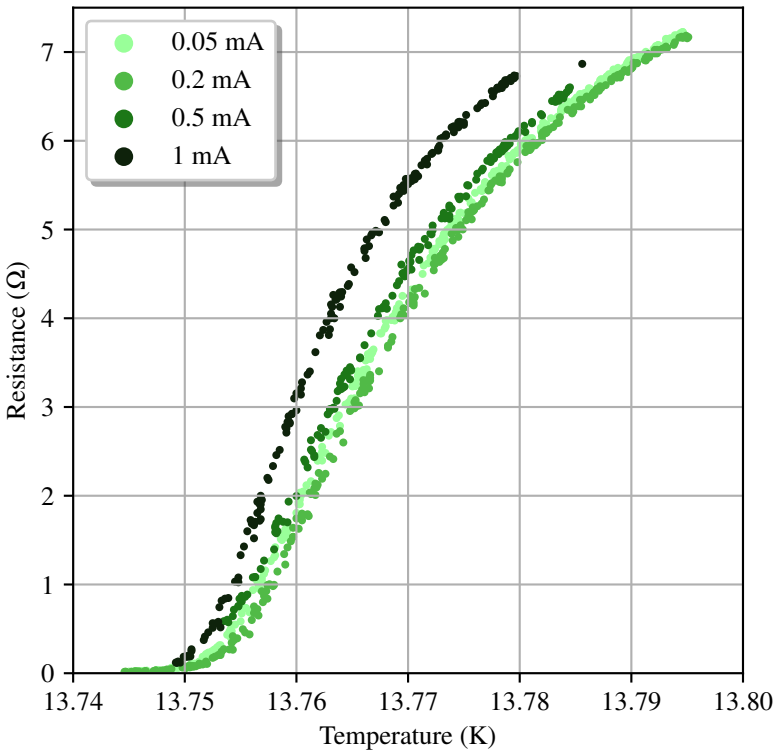

Figure 11: Effect of excitation current on superconducting transition of sample C. Ramp rate $\sim 1.6 \times 10^{-5}$ K s^{-1}. All temperature sweeps are from low to high temperature.

Current (mA)	T_C (K)	T_{90} (K)	T_{10} (K)	Transition width (K)
0.05	13.774 ± 0.001	13.879 ± 0.001	13.757 ± 0.001	0.122 ± 0.001
0.2	13.775 ± 0.001	13.879 ± 0.001	13.758 ± 0.001	0.121 ± 0.001
0.5	13.773 ± 0.001	13.874 ± 0.001	13.756 ± 0.001	0.118 ± 0.001
1	13.768 ± 0.001	13.866 ± 0.001	13.754 ± 0.001	0.112 ± 0.001

Table 5: Superconducting transition temperatures and transition widths for sample C at different excitation currents. The same lines as in figure 4 are used to determine the T_{90}, T_{50} and T_{10} values for each current.

About TeslatronPT Plus

TeslatronPT Plus is an open-architecture low-temperature measurement system that builds on Quantum Design Oxford's proven cryogen-free low-temperature and superconducting magnet technology. It offers fully automated control of temperature and magnetic field parameters, with integrated data logging within our software environment. The system seamlessly integrates with measurement instrumentation, such as that from Lake Shore (the M81 & M91) and other third-party devices, so is easily configurable across experimental setups.

With open-source Python measurement scripts **Teslatron**PT Plus simplifies instrument management, enabling automated measurement sequences and secure data handling. Combining advanced hardware with powerful software tools, it delivers a simple, flexible, and future-proof solution for electrical transport measurements at low temperatures and in high magnetic-fields.

Find out more about Quantum Design Oxford - **Teslatron**PT Plus